Society of Petroleum Engineers

SPE-187165-MS

Nanoparticle-Stabilized Foams for High-Temperature, High-Salinity Oil Reservoirs

Robin Singh and Kishore K. Mohanty, The University of Texas at Austin

This paper was prepared for presentation at the SPE Annual Technical Conference and Exhibition held in San Antonio, Texas, USA, 9-11 October 2017.

Abstract

The goal of this work is to develop foams stabilized by a combination of nanoparticles and surfactants for high-temperature, high-salinity reservoirs. Two types of silica nanoparticles (LNP1, LNP2) with different grafted low molecular weight ligands/polymers were used. First, aqueous stability tests of these formulations were performed at high-temperature (80 °C) and high-salinity conditions (8 wt% NaCl and 2 wt% $CaCl_2$). The screened nanoparticles were used in combination with a surfactant. Second, bulk foam tests were performed to evaluate their foaming performance in bulk. Finally, oil displacement experiments were conducted in an in-house, custom-built 2D sand pack with flow visualization. The sand pack had two layers of silica sand — top layer with 40-70 mesh and bottom layer with 100-120 mesh, which resulted in a permeability contrast of 6:1. Water flood with subsequent foam flood was performed. The grafting of low-molecular-weight polymers/ligands on silica nanoparticle surfaces resulted in steric stabilization under high-temperature and high-salinity conditions. In the oil displacement experiments in the layered sand packs, the water flood recoveries were low (~33% OOIP) due to channeling in the top high-permeability region, leaving the bottom low-permeability region completely unswept. Foam flooding with just the surfactant leads to a drastic improvement in sweep efficiency. It resulted in an incremental oil recovery as high as 43.3% OOIP. Different cross-flow behaviors were observed during foam flooding. Significant cross-flow of oil from low-permeability region to high-permeability region was observed for the case of surfactant. Conversely, the LNP2-surfactant blend resulted in no crossflow from the low permeability layer with complete blocking of the high-permeability region due to the formation of in-situ emulsion. Such selective plugging of high-perm channels via nanoparticles with optimum surface coating has significant potential in recovering oil from heterogeneous reservoirs.

Introduction

Gas enhanced oil recovery is one of the widely applied EOR methods. The displacement efficiency of gas injection is excellent, if the reservoir pressure is above the minimum miscibility pressure where gas is completely miscible with oil (Orr, 2007). However, due to inherent low viscosity and density of gases, gas injection leads to viscous instability and gravity override. Reservoir heterogeneity further contributes to poor volumetric sweep efficiency (Lake et al., 1986). Foam is a promising tool to improve sweep efficiency in

gas floods (Rossen, 1996). It can reduce the mobility of gas by several orders of magnitude by increasing the apparent viscosity of gas (Hirasaki and Lawson, 1985) while the liquid phase mobility remains unchanged (Eftekhari and Farajzadeh, 2017). Moreover, gas trapping further reduce the gas mobility during foam flow in porous media (Tang and Kovscek, 2006). The concept of foam was first introduced by Boud and Holbrook in 1958. Since then, several successful foam field trials has been reported (Hoefner et al., 1995; Rossen et al., 2017; Skauge et al., 2002).

Foam stability under high-temperature and/or high-salinity (HTHS) conditions is quite challenging because of two main reasons. First, foam strength typically decreases with increase in temperature. This is because of reduction of liquid phase viscosity at higher temperatures, which expedites the liquid drainage process in foam lamellae. Second, the aqueous stability of surfactants limits their use under HTHS conditions. Several researchers have investigated novel surfactant-stabilized foams for HTHS conditions. Chen et al. (2015) reported CO_2-in-water (C/W) foam using a non-ionic surfactant with a high degree of ethoxylation. Similarly, Cui et al. (2016) studied Ethomeen C12 surfactant-stabilized C/W foam for HTHS applications in carbonates. This surfactant was only stable at lower pH (close to 4) as it required complete protonation of C12 to be soluble. Xue et al. (2015) reported viscous C/W foams at a high salinity of 14.6% TDS brine at 120 °C using CO_2-soluble ionic surfactants. Recently, Alzobaidi et al. (2017) reported highly stable C/W foams of viscosity more than 100 cp using zwitterionic surfactants at 120 °C. The high apparent viscosity of the foam was attributed to the viscoelastic nature of the surfactant. Such surfactant-stabilized foams could potentially be made more robust using nanoparticles with specific surface coatings.

In the last decade, there is a recent surge in the research of nanomaterials for oilfield applications. It includes use of nanoparticle in Foam EOR (Emrani et al., 2017; Kim et al., 2016; Singh et al., 2015), nanofluid EOR (Hendraningrat et al., 2013; Zhang et al., 2014), hydraulic fracturing fluids (Barati et al., 2012), wettability alteration (Karimi et al., 2012) and drilling fluids (Zakaria et al., 2012). One of the advantages of nanoparticles is that they could be grafted with different functional groups to impart desirable characteristics for subsurface applications. These include viscosity increment (Ponnapati et al., 2011), improved aqueous stability (Griffith and Daigle, 2017), and desired surface-wettability (Panthi et al., 2017). It makes the nanoparticles quite lucrative for oilfield applications. However, colloidal stability of nanoparticles under high temperature and high salinity conditions is a challenge. According to the Derjaguin–Landau–Verwey–Overbeek (DLVO) theory, the sum of attractive van der Waals (vdW) forces and repulsive electrostatic forces dictates the stability of the nanoparticles (Israelachvili, 2015). The presence of high amount of monovalent and divalent ions screens the inherent charges on nanoparticles, which reduces the electrostatic repulsion between particles. The Debye length, which is a measure of the distance over which the electrostatic repulsion is felt in the solution, decreases with an increase in salinity (Eslahian et al., 2014). For example, for a salinity of 150 mM, the Debye length is only 0.8 nm (Jiang et al., 2009). In such cases, nanoparticles aggregate due to the van der Waals forces (Elimelech et al., 2013). Moreover, if the nanoparticles are negatively charged such as bare silica nanoparticles at pH 7, the presence of oppositely charged ions such as Ca^{+2} could result in interparticle bridging which expedites the nanoparticle aggregation (Wuelfing et al., 2001).

Several approaches can be adopted to stabilize nanoparticles under harsh conditions. One such approach is steric stabilization which involves grafting macromolecules or ligands on the nanoparticle surface (Worthen et al., 2016; Yang and Liu, 2010). The presence of these ligands results in steric hindrance, which reduces the probability of two nanoparticles to collide or interact. Additionally, the ligands should have the ability to solvate under the given harsh conditions in aqueous media and form hydration shell around the nanoparticles. Such ligands can provide steric stabilization to the core nanoparticles (Napper, 1983).

In our previous study (Singh and Mohanty, 2015), we reported the synergistic effects of the mixture of hydrophilic silica nanoparticles and anionic surfactant on foam stabilization in both bulk and homogeneous porous media. We demonstrated that as the concentration of nanoparticles increases, the mobility reduction

factor of surfactant-NP foam in homogeneous Berea core increases up to a factor of two. Recently, we showed that such synergy is even more pronounced in a heterogeneous layered sand pack system by performing visualization experiments (Singh and Mohanty, 2017). These experiments allowed us to identify different cross-flow behavior governing the foam flow in such heterogeneous media such as flow diversion from high-perm to low-perm regions (Ayesh et al., 2017). In this work, the first objective was to investigate the stability of two types of silica nanoparticles (grafted with different ligands) under high-temperature and high-salinity conditions. The screened nanoparticle system was then evaluated as a foam stabilizer in bulk and porous media. Finally, we evaluated and visualized the foaming performance of ligand-grafted nanoparticles along with anionic surfactant in layered, heterogeneous sand packs.

Methodology

Materials

Two different types of surface-modified silica nanoparticles were used in the study. These nanoparticles were coated with two different low-molecular-weight ligands - polyethylene glycol and (3-Glycidyloxypropyl)trimethoxysilane, (GLYMO). These nanoparticles are referred in this paper as LNP1 and LNP2. The sizes of LNP1 and LNP2 in DI water at pH 7 were 20 and 12 nm, respectively. An anionic surfactant with a sulfonate head group (68% active) was used in these experiments. Sand (US Silica) of two different mesh sizes, 100-120# and 40-70#, were used to prepare heterogeneous sand packs. Crude oil was obtained from a reservoir, and it had a viscosity of 32 cp at 25 °C and density of 0.825 g/cm^3. The viscosity was measured using an AR-G2 rheometer from TA instruments. Sodium chloride (Fisher Chemical), calcium chloride (Sigma-Aldrich) and nitrogen (research grade, Matheson) were used as received. Ultrapure water with a resistivity greater than 18.2 MΩ-cm was used to prepare brine solutions. The zeta-potential of nanoparticles solutions were characterized with a Delsa Nano analyzer.

Aqueous Stability of Nanoparticles and Surfactants

The aqueous stability of nanoparticles or surfactant solutions were evaluated under varying salinity conditions at three different temperatures 25, 60 and 80 °C. To prevent evaporation of the samples, custom-made borosilicate glass vials were used. These vials were sealed from the top using Teflon-threaded caps and chemical-resistant O-rings. 10 ml of 0.5 wt% nanoparticles solution with varying salinity (of 1 to 8 wt % NaCl and API brine) were taken in the vials and placed in different ovens operating at 25, 60 and 80 °C. The aqueous stability of the samples was monitored visually for two months.

Bulk Foam Stability

The morphology of foam flowing in bulk is different from foam in porous media. The bubble sizes of foam, which is a key foam characterization parameter, in bulk is the order of magnitude smaller than the size of the medium holding it, whereas the bubble sizes are similar to pore sizes for the cases of foam flow in porous media. Albeit these differences, bulk foam stability tests are often conducted as a basic screening tool to compare and evaluate foaming tendency of different formulations (Singh and Mohanty, 2016a). One of such common tests is the static foam test in which decay of foam volume with time is monitored (Singh and Mohanty, 2016b). In this work, bulk foam stability of nanoparticle-surfactant mixtures is evaluated at 25 °C and 80 °C. The salinity of the system was kept constant; API brine (8wt% NaCl + 2wt% $CaCl_2$) was used. A 10-ml sample was taken in a glass vial and was sealed using a PTFE-lined cap. The sample was kept in an oven for more than 3 hours to attain thermal equilibrium before making foam. The vial was hand shaken vigorously for 15 seconds to generate foam. The foam height (above the drained liquid phase) was recorded as a function of time.

Preparation of 2D Heterogeneous Sandpack

Foams can divert flow from high permeability regions to low permeability regions in heterogeneous porous media. The foam flow phenomenon in a heterogeneous medium is much complex as compared to foam flow in 1D, homogenous system such as cores which are typically studied in the literature. To understand and visualize the foam flow dynamics in a heterogeneous medium, a simplified layered sand pack model was fabricated. An in-house sand pack holder made of stainless steel was designed with one face made of a transparent plate (thickness: 0.75 inches) for visualization. The dimension of the interior of the holder was 5.4 inch × 2.9 inch × 1 inch. There were three injection ports on the left side and three production ports on the right side, as shown in Figure 1. Stainless steel screens (400 mesh) were welded on these ports to prevent sand flow. The holder was packed with two layers of silica sand: the top layer using 40-70 mesh and the bottom layer using 100-120 mesh. The permeability of the top layer was 22.6 Darcy while that of the bottom layer was 3.8 Darcy. Thus, the permeability contrast was about 6:1. The layer permeability was measured by flowing water through a 1D tube (1 ft long; 1 inch in diameter) packed with each sand. The permeability and the porosity of the two-layer system were measured to be 15.7 Darcy and 31%, respectively.

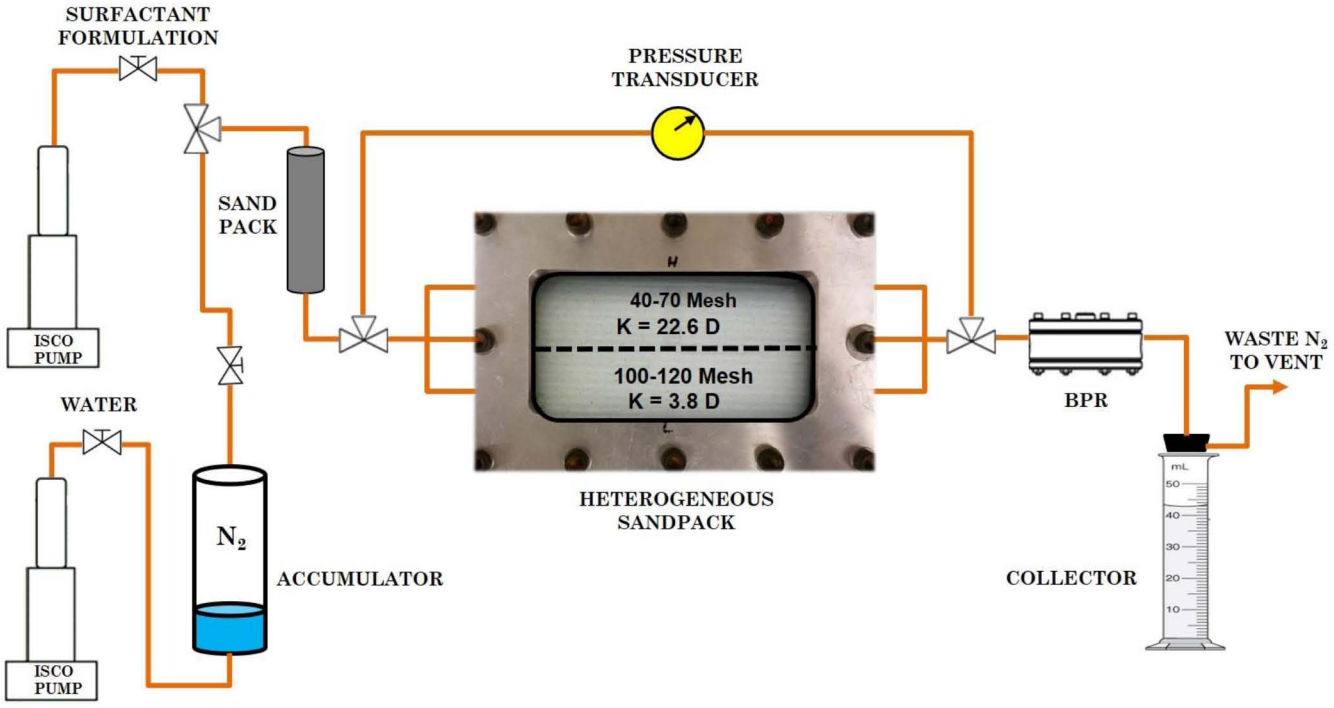

Figure 1—Schematic of the apparatus for oil displacement experiments

Oil Displacement Experiments

Foam flow experiments were conducted to investigate the dynamics of foam flow in a heterogeneous porous medium in the presence of reservoir crude oil. Foams were stabilized by either a surfactant or a surfactant-nanoparticle blend. Petrophysical properties such as porosity and permeability of the sand pack were determined before performing the vacuum saturation with crude oil. The conventional technique of oil saturation is to displace the brine-saturated porous media with crude oil at a constant high pressure. However, due to the high permeability contrast (6:1) in the present system, it was not possible to achieve high initial oil saturation using this technique. Therefore, the initial oil saturation was obtained by vacuum saturation which resulted in 100% initial oil saturation for every case.

Figure 1 shows the experimental schematic. Two series-D syringe pumps from Teledyne ISCO (Lincoln, NE) were used in the setup which is capable of low injection rates (as low as 0.001 cc/min). The apparatus was built to co-inject nitrogen gas and aqueous (brine/surfactant/surfactant-nanoparticle blend) solution

through a sand pack (0.6-inch diameter and 6-inch long) to ensure proper mixing and foam generation. The pre-generated foam was then injected through the three ports on the left side of the heterogeneous sand pack. The downstream pressure of the experiment was maintained by a back-pressure regulator (Equilibar, NC and Swagelok, OH) at 110 psi which was installed downstream of the sandpack. The experiment was performed at the room temperature. After the crude oil saturation, the whole setup was pressurized with a back pressure of 110 psi and more than 0.5 PV of oil was injected. The brine flood was then conducted at 10 ft/D for 4 PV until no oil was produced. Nitrogen gas and surfactant or surfactant-NP blend were then co-injected through the foam generator to make a foam of 80% quality (volume fraction of gas). This foam was injected into the two-layer sand pack at an average interstitial velocity of 4 ft/D. This pre-generated foam was injected through the ports on the left side of the heterogeneous sandpack for more than 20 PV. Oil recovery and pressure drops were monitored at each step. The displacement of crude oil by injection fluid was captured using a microscope. The pressure drop across the 2D sandpack was measured using Rosemount differential pressure transducers. An automated data acquisition system (LabView, National Instruments) was used to record the pressure.

Results

Aqueous Stability of Nanoparticles and Surfactants

First, the aqueous stability of two different nanoparticles was evaluated under varying salinity conditions at three different temperatures 25, 60 and 80 °C. Figure 2 shows the stability of both the nanoparticles. Both nanoparticles were stable for the wide range of salinity at room temperature (25 °C). The stability and salt tolerance of both nanoparticles decreased with an increase in the temperature. LNP1 was found stable only below 2 wt% NaCl and 1 wt% NaCl salinity at 60 °C and 80 °C, respectively. At higher salinities, precipitation of the nanoparticles was observed indicating severe aggregation. However, LNP2 was found to be more stable than LNP1 with a salt tolerance of 8 wt% at 60 °C and 2 wt% at 80 °C. This shows that the GLYMO surface coating was more efficient than PEG surface coating in providing steric stabilization of the silica nanoparticles under high salinity. Based on these results, LNP2 nanoparticles were chosen in the subsequent experiments. Note that the pH of the LNP2 solutions was 8.5 and was not modified in this test.

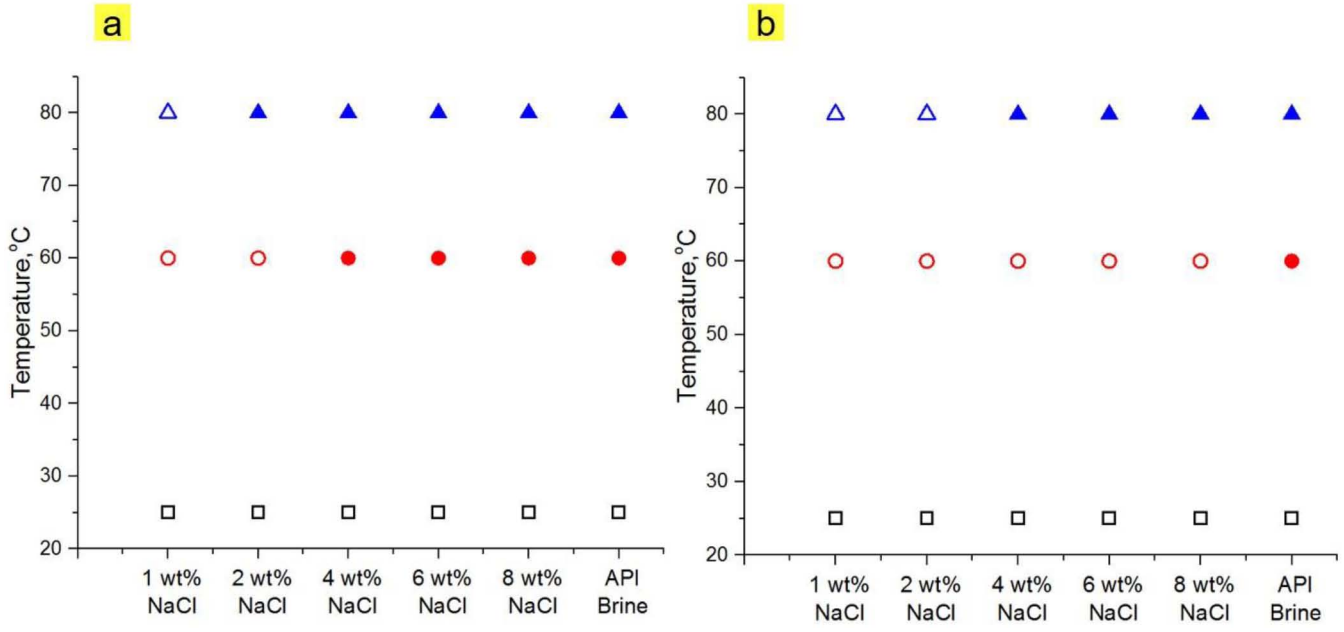

Figure 2—Aqueous stability of (a) LNP1 and (b) LNP2 at different temperatures and varying salinity: hollow markers and filled markers represent clear solution and precipitation, respectively.

The LNP2 nanoparticles are highly negatively charged under natural pH of 8.5 as confirmed via zeta potential measurements. A decrease in surface charge (less negative) of the nanoparticle (to a limit) is desirable as it would reduce the interaction with the divalent ions and thus increasing stability and salt tolerance of the system. A decrease in pH of the solutions is expected to reduce the surface charge of the system and hence can increase the stability of the nanoparticles. Therefore, the pH of LNP2 solutions was varied from 8.5 to 2. The salinity of the solutions was kept constant and equal to API brine (8 wt% NaCl and 2 wt% $CaCl_2$) which represents a high salinity brine with high hardness. Figure 3 shows the results of the aqueous stability of the nanoparticles after two months. The solutions were found to be completely clear for the cases of pH 2 and 3.5 at the three temperatures. For pH 5 and 6.5, cloudy solutions were observed indicating some aggregations of nanoparticles at 60 and 80 °C. For higher pH such as 7 and 8.5, precipitations of nanoparticles were observed indicating poor aqueous stability at 60 and 80 °C.

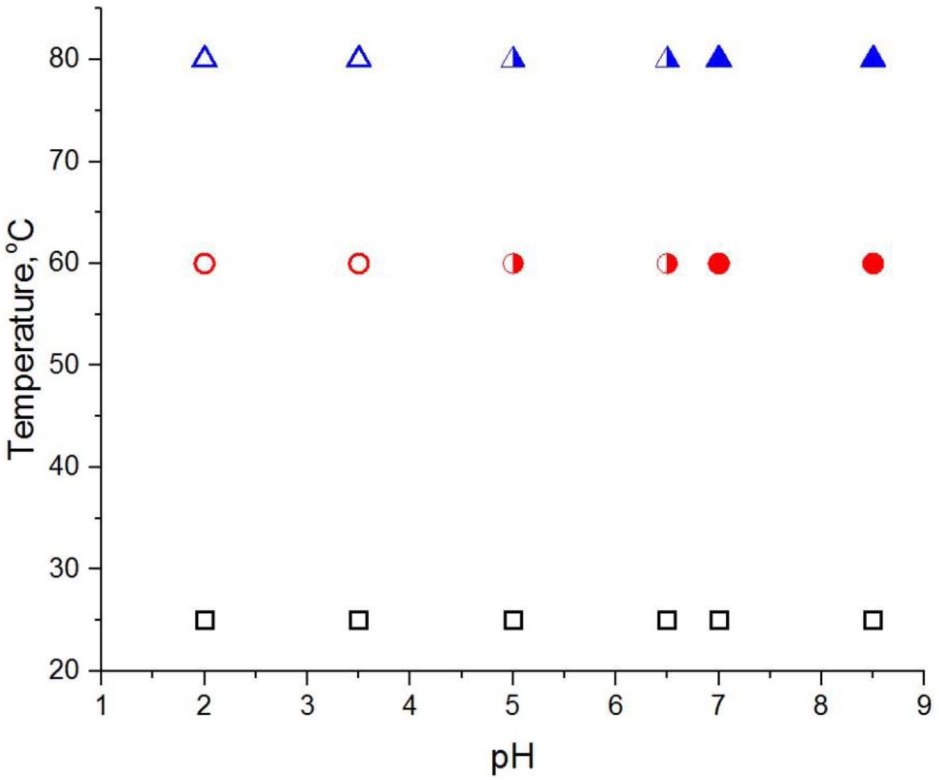

Figure 3—Aqueous stability of LNP2 at varying pH and constant API brine salinity (8 wt% NaCl + 2wt% $CaCl_2$). The hollow markers, semi-filled markers, and filled markers represent a clear solution, cloudy solution, and precipitation, respectively.

Zeta potential of the LNP2 system was then measured as a function of pH to better understand this stability trend. The zeta potential of these nanoparticles at their natural pH of 8.5 was −30 mV. As the pH of the solution was reduced, the magnitude of zeta potential was reduced (becomes less negative) from −30 to −7 mV corresponding to pH 8.5 and 2, respectively, as shown in Figure 4. Such reduction in particle charge reduces the interaction with divalent ions such as Ca^{+2} and increases nanoparticle stability. For very high salinity and high temperature conditions, these nanoparticles are stable at low pH < 3.5. The equilibrium in-situ pH of the reservoir fluids during carbon dioxide flooding are reported to be less than 4. Thus, these nanoparticles could be used to stabilize carbon dioxide-in-water foams under reservoir conditions.

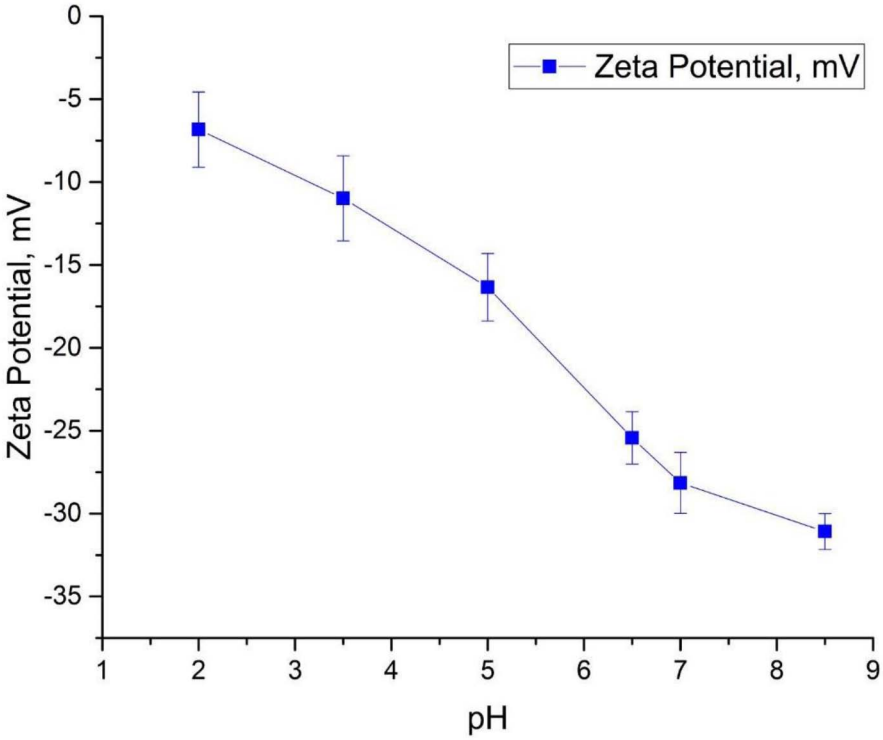

Figure 4—Zeta potential of LNP2 as a function of pH

Bulk Foam Stability

Based on the aqueous stability results, the LNP2 nanoparticles were chosen for further foam studies in bulk and porous media. Static foam test is the most common bulk foam stability tests. Recently, Jones et al. (2016) reported a good correlation between bulk foam stability and apparent foam viscosity in the absence of oil. The LNP2 nanoparticles, when mixed in a vial in the presence of air, does not have any affinity to form foam irrespective of the salt concentration. It is due to the hydrophilic nature of the nanoparticles (even though the coating has small hydrophobic chains). Therefore, to stabilize foam, an anionic surfactant was used in addition. The objective of the static foam tests in the present study was to investigate an optimum surfactant concentration, if any, to be used in the blend of LNP2 and surfactant blend. In this test, the total nanoparticle concentration was kept constant at 0.5 wt%, and salinity was API brine. The surfactant concentration was varied from 0 wt% to 1 wt%. A small amount of blend was taken in a glass vial and was shaken vigorously for 15 seconds to make static foam. The decay in foam height was recorded at 25 ° C and 80 °C.

Figure 5 shows the static foam in the vials with varying concentration of surfactant at time t = 0 minutes. Figure 5a shows the vial with only 0.5 wt% LNP2 nanoparticles solutions. It can be seen that nanoparticles alone show negligible foaming tendency. The initial foam height, which is often referred in the literature as foamability, increases with the increase in surfactant concentration. Note that the CMC of this surfactant is close to 0.125 wt% as measured in a previous study (Panthi et al., 2017). Figure 6 shows the decay of foam heights at 25 °C (Figure 6a) and 80 °C (Figure 6b). The foam heights were normalized with respect to maximum possible height (which is the maximum foam height for the case of 1 wt% surfactant at t=0 minutes) to obtain relative foam height. Several observations can be made from the plots. Foam strength increases monotonically with the increase in surfactant concentration and no optimum surfactant concentration was observed for foam stability as evident from foamability as well as foam decay behavior. Note that the decay of foam was increased significantly at the higher temperature of 80 °C as compared to 25 °C. Based on this test, a surfactant concentration of 0.5 wt% was chosen for foam flooding in the subsequent oil displacement experiments.

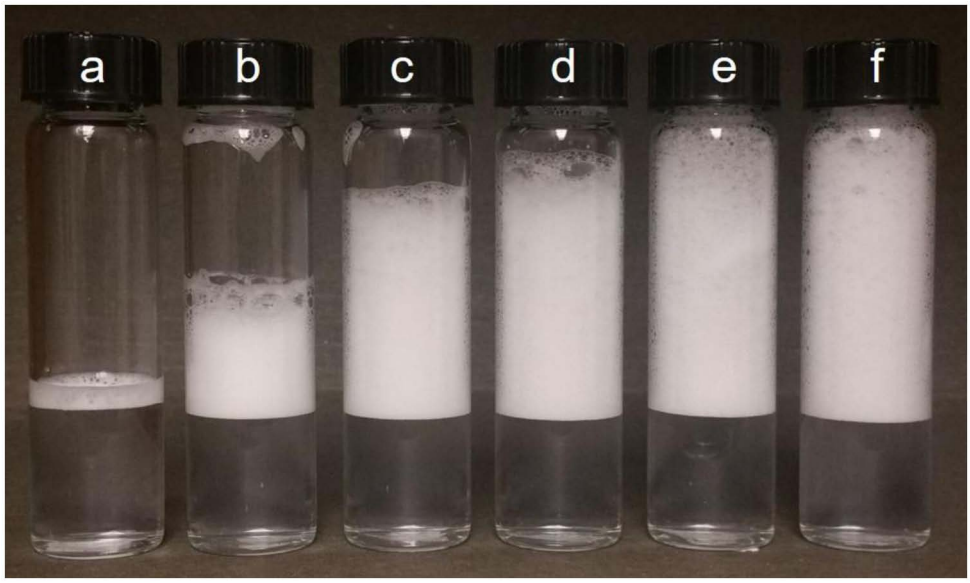

Figure 5—Static foam at time t = 0 min at 25 °C formed using 0.5 wt% LNP2 nanoparticles and increasing concentrations of surfactant. The concentration of surfactant was (a) 0 wt%, (b) 0.0625 wt%, (c) 0.125 wt%, (d) 0.25 wt%, (e) 0.5 wt %, and (f) 1 wt%. The salinity was constant in each sample and equal to API brine (8 wt% NaCl and 2 wt% $CaCl_2$)

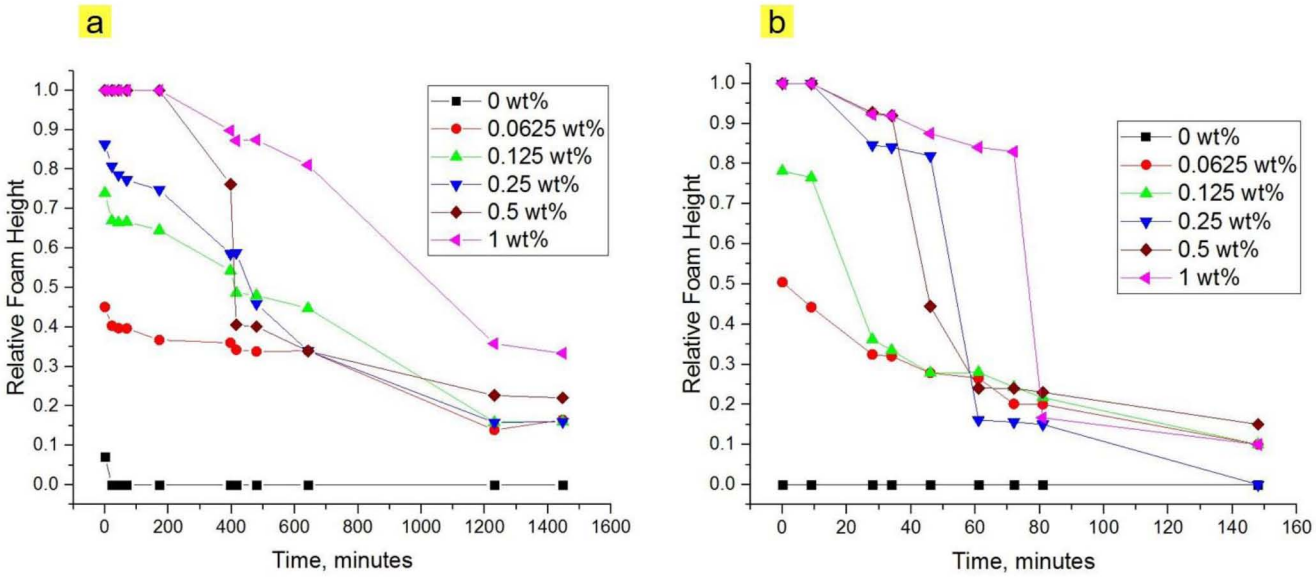

Figure 6—Static foam test with formulations containing 0.5 wt% LNP2 nanoparticles and varying concentration of surfactant at (a) 25 °C and (b) 80 °C. The salinity was constant in each sample and equal to API brine (8 wt% NaCl and 2 wt% $CaCl_2$)

Oil Displacement Experiments

The oil displacement experiments were performed to evaluate and visualize foaming performance of the surfactant and the surfactant-nanoparticle mixture under high salinity conditions. Since the visualization required the use of transparent acrylic sheet whose pressure/temperature rating was not very high, the experiments were performed under low pressure (~110 psi) and room temperature. As high-pressure CO_2, which would have yielded an equilibrium pH<4, could not be used, the pH of the aqueous phase was adjusted using a weak acid. Before conducting the oil displacement experiments, another independent experiment was performed in which API brine of pH 3.5 was injected in a brine-saturated (pH 7) sandpack. When HCL was used to lower the pH of the injection brine, the effluent pH was found to be close to 5.5 even after several pore volumes of injection. This was possibly because of strong reactivity of HCL acid with the

minerals present in sand grains. However, when citric acid was used, the pH was able to propagate along the sand pack, and the effluent pH was found to be 3.5. Therefore, in these experiments, citric acid was used to adjust the pH.

Flood 1 was conducted with the surfactant as the foaming agent. The sandpack was vacuum-saturated with crude oil which resulted in the initial oil saturation of 100%. Figure 7 shows the injection schedule, cumulative oil recovery (secondary y-axis) and overall pressure drop (primary y-axis) across the sandpack. First, brine flood was conducted at 10 ft/D to mimic a waterflood in a reservoir. It was continued for more than 4 PV until no oil was produced. The pH of injected brine was adjusted to 3.5 using citric acid. The waterflood oil recovery was 33.6 %OOIP (original oil in place), and oil saturation was reduced to 66.4%. The pressure drop during water flood was very low (0.04 psi). The oil recovery during this stage was low due to channeling of injected brine from the top high permeability layer. Note that the permeability contrast between the top and bottom layer was 6:1. Figure 8a shows the oil displacement profile after 4 pore volume of brine injection. Although the mobility ratio of brine (1 cp) displacing oil (32 cp) is unfavorable, the sweep in the top layer was good (visually), as seen from the Figure 8a, because of the high permeability of the layer. The pH of the effluent was tested at the end of water flood, and it was close to 3.5. Then, foam flooding was performed at 4ft/D using the anionic surfactant as the foaming agent. The formulation has 0.5 wt% surfactant in API brine. The pH was lowered to 3.5 using the citric acid. The foam quality (volume fraction of gas) was kept constant at 80%.

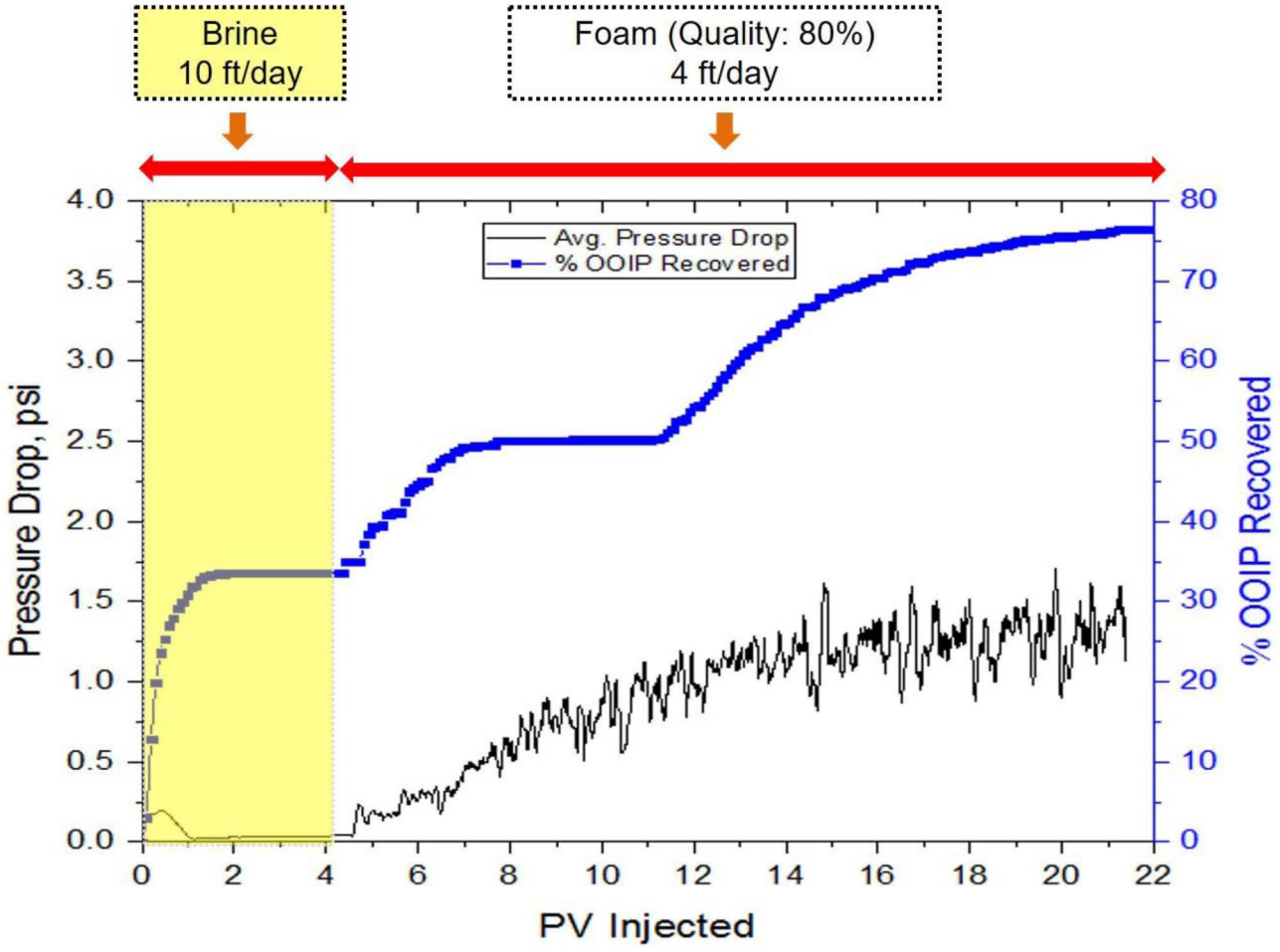

Figure 7—Pressure drop profile (black, left axis) and cumulative oil recovery (blue, right axis) for Flood 1

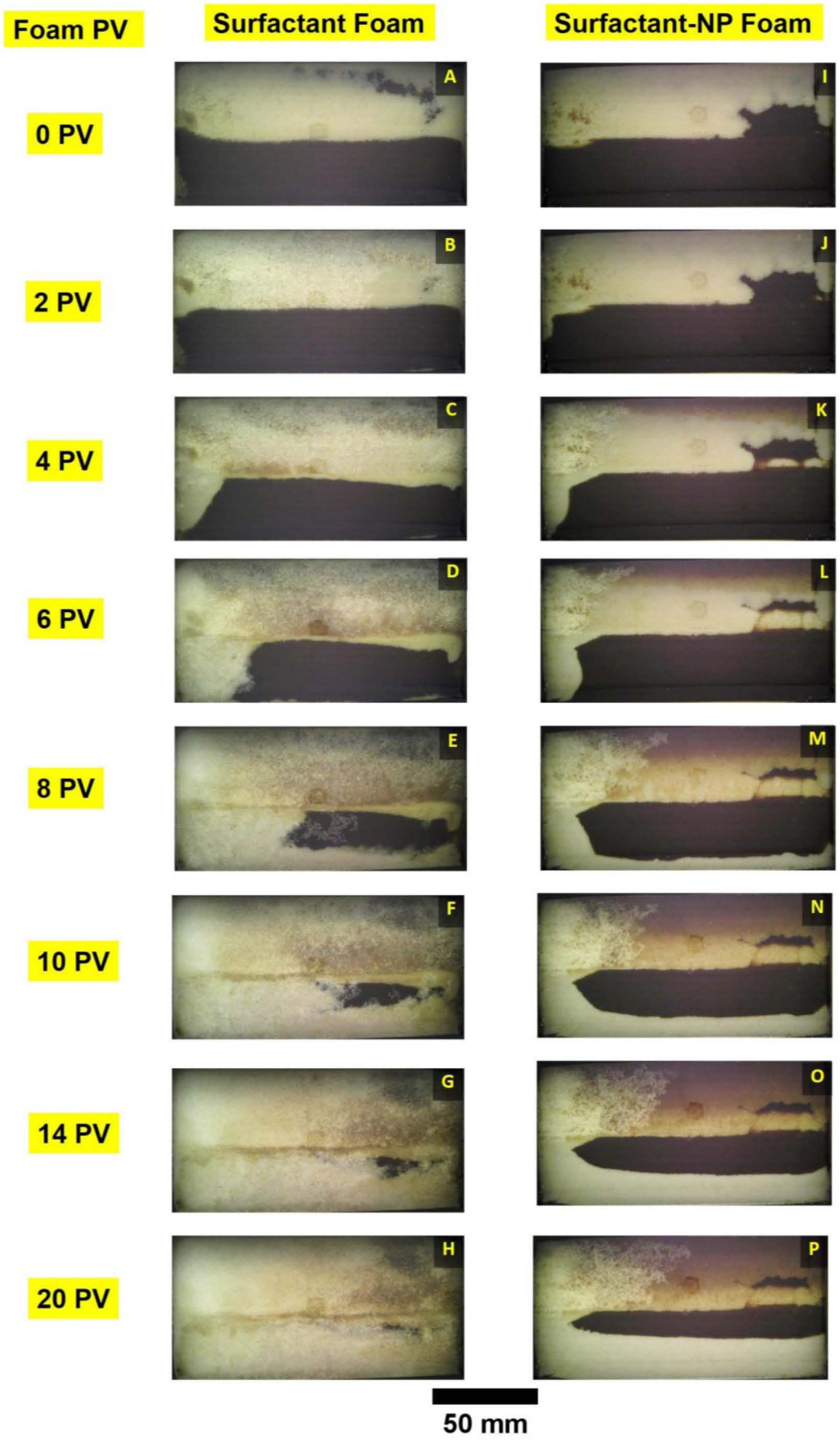

Figure 8—Oil distributions during Flood 1 (A to H) and Flood 2 (I to P) at different pore volumes of foam injection

Figure 8 B-H shows the oil displacement profiles during foam injection; injected foam PV is indicated (does not include water flood). In the first 2 PV of foam injection, the foam only swept the top layer only (Figure 8b) and recovered about 11.5 % OOIP oil. It is to be noted that the even though the top layer looked clean after brine flood visually, it has a significant amount of residual oil left which was recovered by foam in the first 3 PV (7 PV including water flood). The pressure drop during this stage increased (as compared to brine injection) indicating an increase in apparent foam viscosity. Figure 8C shows how foams start diverting injection fluid from the high permeability layer to the low permeability layer. The displacement in the lower layer is almost piston-like at 6 PV foam injection (Figure 8D). The oil from the lower layer moves into the upper layer without much oil production from the cell during 4-8 PV foam injection. This cross-flow behavior has been typically observed during foam flow in heterogeneous systems and has been reported in a previous study (Singh and Mohanty, 2017). The oil pushed into the upper layer is eventually produced between 8 and 14 PV of foam injection. The foam flood was continued for more than 18 PV. The pressure drop across the sand pack increased to 1.4 psi by the end of the experiment. The ultimate cumulative oil recovery was 76.9 %OOIP, the incremental oil recovery by foam was 43.3 %OOIP, and the final oil saturation was 23.1%. The foam tends to generate easily in the high permeability layer and blocks it due to the formation of viscous foams. This shows the self-regulating capabilities of foam which make it lucrative as a conformance control tool in a heterogeneous system such as the present one.

In Flood 2, we wanted to explore the potential synergism of using the LNP2 nanoparticles with the anionic surfactant. The sand pack was again packed with clean, dry sand in a similar way as before and was vacuum-saturated with crude oil with an initial saturation of 100%. After an initial water flood, a foam flood was conducted using a mixture of the surfactant (0.5 wt%) and LNP2 nanoparticles (0.5% LNP2) as the foaming agent. The formulation was prepared in API brine (8 wt% NaCl and 2 wt% $CaCl_2$) with a pH of 3.5. Figure 9 shows the injection procedure, cumulative oil recovery (secondary y-axis) and overall pressure drop (primary y-axis) across the sandpack.

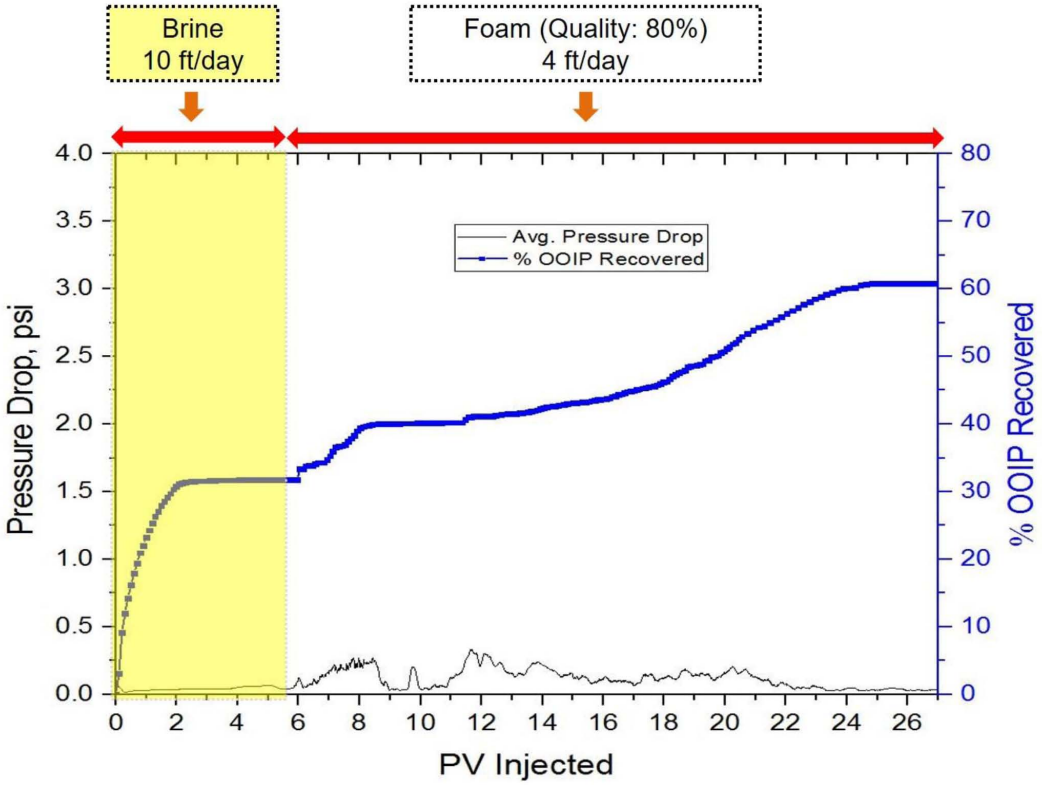

Figure 9—Pressure drop profile (black, left axis) and cumulative oil recovery (blue, right axis) for Flood 2

Similar to Flood 1, first a brine flood was conducted at 10 ft/D. It was continued for more than 5 PV. The brine flood oil recovery was 31.7 %OOIP, and oil saturation was reduced to 68.3 % which is similar to the Flood 1. Then, nanoparticle-surfactant solutions and nitrogen gas were coinjected with a quality of 80% at 4 ft/D. Figure 8 shows the comparison of oil distribution due to foam flooding at different pore volumes (PV) of foam injection for the surfactant case (left) and the blend case (right). The initial oil displacement process by the blend foam (<6 PV) was similar to the surfactant case in Figure 8 (A-D vs. I-L). The foam first swept the high permeability layer resulting in 10 %OOIP additional oil recovery where as the corresponding recovery in Flood 1 was 20 %OOIP. The pressure drop during this stage increased to 0.2 psi compared to 0.04 psi during waterflood. (Note that brine flood was performed at 2.5 times faster rate). The cross-flow of foams from high permeability to low permeability was clearly evident from Figure 8 K-M. However, during this flood, no cross-flow of oil from low-permeability layer to high-permeability was observed as opposed to the surfactant foam case, as shown in Figure 10. The flow in the high permeability layer was completely blocked. This could be due to formation nanoparticle-assisted oil-water emulsions. The foam flood, in this case, was continued for more than 21 PV. The ultimate cumulative oil recovery was 60.8 %OOIP, the incremental oil recovery by foam was 29.0 %OOIP, and the final oil saturation was 39.2 %. The pressure drop never built up above 0.25 psi in Flood 2, much lower than about 1.2 psi in Flood 1.

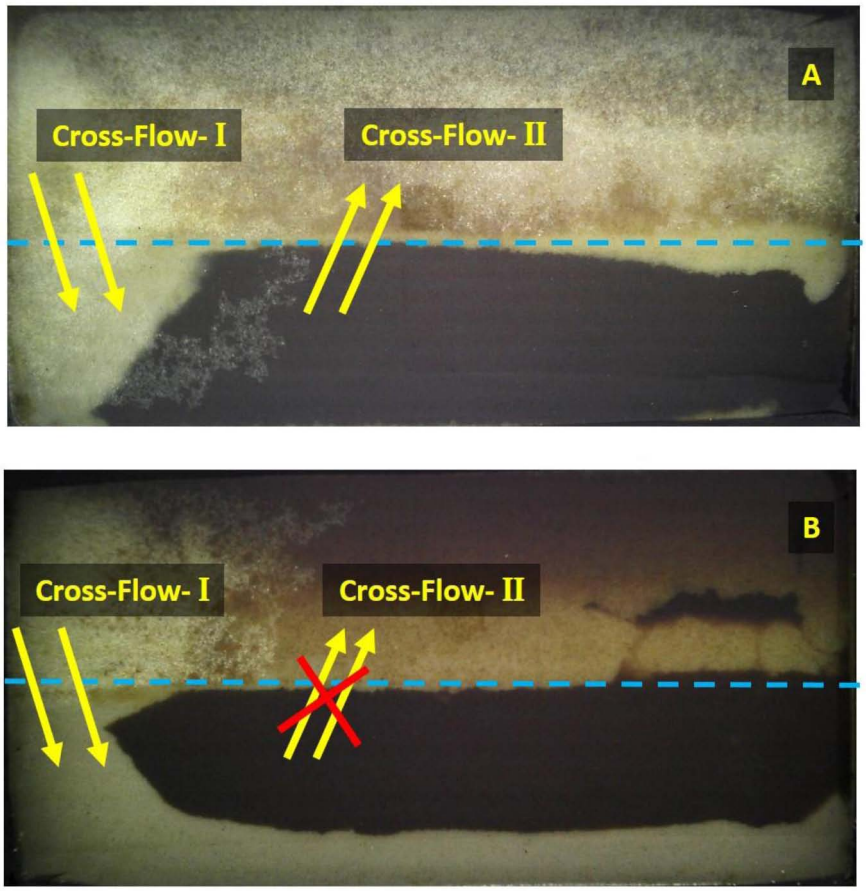

Figure 10—Cross-flow mechanisms observed during oil displacement experiments

Although the final recovery in the LNP2-surfactant blend case was low, it resulted in selective plugging of the high permeability layer which is desirable in the field applications. Such flow behavior was not observed when hydrophilic silica nanoparticles were used in our previous study (Singh and Mohanty, 2017). It shows that nanoparticle surface-coating can alter foam flow dynamics in heterogeneous porous media. A detailed understanding of the mechanism of emulsion generation via nanoparticles in the particular region would

allow one to design and optimize the surface coating of silica nanoparticles. Such tailored surface-modified nanoparticles show immense potential to act a foam EOR agent under harsh reservoir conditions such as high temperature and high salinity conditions.

Conclusions

The following conclusions can be drawn from this work:

1. The grafting of low-molecular-weight ligands such as polyethylene glycol (PEG) and (3-Glycidyloxypropyl)trimethoxysilane, (GLYMO) on silica nanoparticles resulted in steric stabilization and improved the aqueous stability in both high and low temperatures as compared to bare silica nanoparticles.
2. Silica nanoparticles were sterically stabilized using GLYMO coating under high salinity (API brine) at 80 °C for pH < 3.5. These nanoparticles show no signs of aggregation even after 2 months. The enhanced stability is attributed to the high degree of solvation of GLYMO ligands that remain soluble in the concentrated brine at the high temperature.
3. Foam flood in heterogeneous sand packs with a reservoir crude oil showed that incremental oil recovery of 29.0 % to 43.3% OOIP (over waterflood) using immiscible foams.
4. Despite the presence of a permeability contrast (6:1), which induces channeling of gas through the high-permeability region, the foam was effective in diverting fluid to the low-permeability region even in the presence of crude oil. This crossflow behavior was observed in both cases: foams stabilized by surfactant alone and surfactant-LNP2 mixture.
5. Significant cross-flow of oil from low-permeability region to high-permeability region (L→H) was observed for the case of surfactant foam flood. However, the LNP2 foam flood resulted in no (L→H) crossflow with complete blocking of the high-permeability region possibly due to the formation of in-situ emulsion. Such selective plugging of high-permeability channels via nanoparticles with optimum surface coating could have significant potential in recovering oil from heterogeneous reservoirs.

Acknowledgement

We are thankful to the sponsors of Gas EOR Industrial Affiliates Project at The University of Texas at Austin for partial funding of this work.

References

Alzobaidi, S., Da, C., Tran, V., Prodanović, M., Johnston, K.P., 2017. High temperature ultralow water content carbon dioxide-in-water foam stabilized with viscoelastic zwitterionic surfactants. *J. Colloid Interface Sci.* **488**, 79–91. doi:10.1016/j.jcis.2016.10.054

Ayesh, A., H, A., Salazar, R., Farajzadeh, R., Vincent-Bonnieu, S., Rossen, W.R., 2017. Foam Diversion in Heterogeneous Reservoirs: Effect of Permeability and Injection Method. *SPE J.* doi:10.2118/179650-PA

Barati, R., Johnson, S.J., McCool, S., Green, D.W., Willhite, G.P., Liang, J.-T., 2012. Polyelectrolyte complex nanoparticles for protection and delayed release of enzymes in alkaline pH and at elevated temperature during hydraulic fracturing of oil wells. *J. Appl. Polym. Sci.* **126**, 587–592. doi:10.1002/app.36845

Boud, D.C., Holbrook, O.C., 1958. *Gas drive oil recovery process*. US2866507 A.

Chen, Y., Elhag, A.S., Cui, L., Worthen, A.J., Reddy, P.P., Noguera, J.A., Ou, A.M., Ma, K., Puerto, M., Hirasaki, G.J., Nguyen, Q.P., Biswal, S.L., Johnston, K.P., 2015. CO2-in-Water Foam at Elevated Temperature and Salinity Stabilized with a Nonionic Surfactant with a High Degree of Ethoxylation. *Ind. Eng. Chem. Res.* **54**, 4252–4263. doi:10.1021/ie503674m

Cui, L., Ma, K., Puerto, M., Abdala, A.A., Tanakov, I., Lu, L.J., Chen, Y., Elhag, A., Johnston, K.P., Biswal, S.L., Hirasaki, G., 2016. Mobility of Ethomeen C12 and Carbon Dioxide (CO_2) Foam at High Temperature/High Salinity and in Carbonate Cores. *SPE J.* **21**, 1,151–1,163. doi:10.2118/179726-PA

Eftekhari, A.A., Farajzadeh, R., 2017. Effect of Foam on Liquid Phase Mobility in Porous Media. *Sci. Rep.* **7**. doi:10.1038/srep43870

Elimelech, M., Gregory, J., Jia, X., 2013. Particle Deposition and Aggregation: Measurement, Modelling and Simulation. *Butterworth-Heinemann*.

Emrani, A.S., Ibrahim, A.F., Nasr-El-Din, H.A., 2017. Evaluation of Mobility Control with Nanoparticle-Stabilized CO_2 Foam. Presented at the SPE Latin America and Caribbean Petroleum Engineering Conference, SPE-185551-MS. doi:10.2118/185551-MS

Eslahian, K.A., Lang, T., Bantz, C., Keller, R., Sperling, R., Docter, D., Stauber, R., Maskos, M., 2014. Characterization of Nanoparticles Under Physiological Conditions, in: Wegener, J. (Ed.), *Measuring Biological Impacts of Nanomaterials, Bioanalytical Reviews*. Springer International Publishing, pp. 1–29. doi:10.1007/11663_2014_10

Griffith, C., Daigle, H., 2017. Stability of polyvinyl alcohol-coated biochar nanoparticles in brine. *J. Nanoparticle Res.* **19**, 23. doi:10.1007/s11051-016-3705-6

Hendraningrat, L., Li, S., Torsæter, O., 2013. A coreflood investigation of nanofluid enhanced oil recovery. *J. Pet. Sci. Eng.* **111**, 128–138. doi:10.1016/j.petrol.2013.07.003

Hirasaki, G.J., Lawson, J.B., 1985. Mechanisms of foam flow in porous media: apparent viscosity in smooth capillaries. *Soc. Pet. Eng. J.* **25**, 176–190.

Hoefner, M.L., Evans, E.M., Buckles, J.J., Jones, T.A., 1995. CO2 Foam: Results From Four Developmental Field Trials. *SPE Reserv. Eng.* **10**, 273–281. doi:10.2118/27787-PA

Israelachvili, J.N., 2015. *Intermolecular and Surface Forces*. Academic Press.

Jiang, J., Oberdörster, G., Biswas, P., 2009. Characterization of size, surface charge, and agglomeration state of nanoparticle dispersions for toxicological studies. *J. Nanoparticle Res.* **11**, 77–89. doi:10.1007/s11051-008-9446-4

Jones, S.A., van der Bent, V., Farajzadeh, R., Rossen, W.R., Vincent-Bonnieu, S., 2016. Surfactant screening for foam EOR: Correlation between bulk and core-flood experiments. *Colloids Surf. Physicochem. Eng. Asp.* **500**, 166–176.

Karimi, A., Fakhroueian, Z., Bahramian, A., Pour Khiabani, N., Darabad, J.B., Azin, R., Arya, S., 2012. Wettability Alteration in Carbonates using Zirconium Oxide Nanofluids: EOR Implications. *Energy Fuels* **26**, 1028–1036. doi:10.1021/ef201475u

Kim, I., Worthen, A.J., Johnston, K.P., DiCarlo, D.A., Huh, C., 2016. Size-dependent properties of silica nanoparticles for Pickering stabilization of emulsions and foams. *J. Nanoparticle Res.* **18**, 82. doi:10.1007/s11051-016-3395-0

Lake, L.W., Johns, R.T., Rossen, W.R., Pope, G., 1986. *Fundamentals of enhanced oil recovery*. Society of Petroleum Engineers.

Napper, D.H., 1983. *Polymeric stabilization of colloidal dispersions*. Academic Press.

Orr, F.M., 2007. *Theory of gas injection processes*. Tie-Line Publications, Copenhagen.

Panthi, K., Singh, R., Mohanty, K.K., 2017. Microencapsulation and Stimuli-Responsive Controlled Release of Particles Using Water-in-Air Powders. *Langmuir*. doi:10.1021/acs.langmuir.7b00149

Ponnapati, R., Karazincir, O., Dao, E., Ng, R., Mohanty, K.K., Krishnamoorti, R., 2011. Polymer-Functionalized Nanoparticles for Improving Waterflood Sweep Efficiency: Characterization and Transport Properties. *Ind. Eng. Chem. Res.* **50**, 13030–13036. doi:10.1021/ie2019257

Rossen, W.R., 1996. Foams in enhanced oil recovery. *Surfactant Sci. Ser.* 413–464.

Rossen, W.R., Ocampo, A., Restrepo, A., Cifuentes, H.D., Marin, J., 2017. Long-Time Diversion in Surfactant-Alternating-Gas Foam Enhanced Oil Recovery From a Field Test. *SPE Reserv. Eval. Eng.* **20**, 1–7. doi:10.2118/170809-PA

Singh, R., Gupta, A., Mohanty, K.K., Huh, C., Lee, D., Cho, H., 2015. Fly Ash Nanoparticle-Stabilized CO2-in-Water Foams for Gas Mobility Control Applications, in: SPE Annual Technical Conference and Exhibition. Houston, Texas, USA, SPE-175057. doi:10.2118/175057-MS

Singh, R., Mohanty, K.K., 2017. Foam flow in a layered, heterogeneous porous medium: A visualization study. *Fuel* **197**, 58–69. doi:10.1016/j.fuel.2017.02.019

Singh, R., Mohanty, K.K., 2016a. Foams with Wettability-Altering Capabilities for Oil-Wet Carbonates: A Synergistic Approach. *SPE J.* **21**, 1126–1139. doi:10.2118/175027-PA

Singh, R., Mohanty, K.K., 2016b. Foams Stabilized by In-Situ Surface-Activated Nanoparticles in Bulk and Porous Media. *SPE J.* **21**, 121–130. doi:10.2118/170942-PA

Singh, R., Mohanty, K.K., 2015. Synergy between nanoparticles and surfactants in stabilizing foams for oil recovery. *Energy Fuels* **29**, 467–479. doi:10.1021/ef5015007

Skauge, A., Aarra, M.G., Surguchev, L., Martinsen, H.A., Rasmussen, L., 2002. Foam-Assisted WAG: Experience from the Snorre Field. Presented at the SPE/DOE Improved Oil Recovery Symposium, SPE-75157-MS. doi:10.2118/75157-MS

Tang, G.-Q., Kovscek, A.R., 2006. Trapped Gas Fraction During Steady-State Foam Flow. *Transp. Porous Media* **65**, 287–307. doi:10.1007/s11242-005-6093-4

Worthen, A., Tran, V., A. Cornell, K., M. Truskett, T., P. Johnston, K., 2016. Steric stabilization of nanoparticles with grafted low molecular weight ligands in highly concentrated brines including divalent ions. *Soft Matter* **12**, 2025–2039. doi:10.1039/C5SM02787J

Wuelfing, W.P., Zamborini, F.P., Templeton, A.C., Wen, X., Yoon, H., Murray, R.W., 2001. Monolayer-Protected Clusters: Molecular Precursors to Metal Films. *Chem. Mater.* **13**, 87–95. doi:10.1021/cm0005440

Xue, Z., Panthi, K., Fei, Y., Johnston, K.P., Mohanty, K.K., 2015. CO2-Soluble Ionic Surfactants and CO2 Foams for High-Temperature and High-Salinity Sandstone Reservoirs. *Energy & Fuels* **29**, 5750–5760. doi:10.1021/acs.energyfuels.5b01568

Yang, X., Liu, Z., 2010. A Kind of Nanofluid Consisting of Surface-Functionalized Nanoparticles. *Nanoscale Res. Lett.* **5**, 1324. doi:10.1007/s11671-010-9646-6

Zakaria, M., Husein, M.M., Harland, G., 2012. Novel Nanoparticle-Based Drilling Fluid with Improved Characteristics. Presented at the SPE International Oilfield Nanotechnology Conference and Exhibition, SPE-156992-MS. doi:10.2118/156992-MS

Zhang, H., Nikolov, A., Wasan, D., 2014. Enhanced Oil Recovery (EOR) Using Nanoparticle Dispersions: Underlying Mechanism and Imbibition Experiments. *Energy & Fuels* **28**, 3002–3009. doi:10.1021/ef500272r